Handb Environ Chem Vol. 5, Part F, Vol. 3 (2005): 97 – 132
DOI 10.1007/b11433

Nonaqueous Phase Liquid Pool Dissolution in Subsurface Formations

Constantinos V. Chrysikopoulos (✉)

Department of Civil Engineering, University of Patras, Rio 26500, Greece
gios@upatras.gr

Abstract The objective of this chapter is to present some recent developments on nonaqueous phase liquid (NAPL) pool dissolution in water saturated subsurface formations. Closed form analytical solutions for transient contaminant transport resulting from the dissolution of a single component NAPL pool in three-dimensional, homogeneous porous media are presented for various shapes of source geometries. The effect of aquifer anisotropy and heterogeneity as well as the presence of dissolved humic substances on mass transfer from a NAPL pool is discussed. Furthermore, correlations, based on numerical simulations as well as available experimental data, describing the rate of interface mass transfer from single component NAPL pools in saturated subsurface formations are presented.

Keywords NAPL pool dissolution · Mass transfer correlations · Cotransport · Mathematical modeling

List of Symbols and Abbreviations

a	Major semi-axis of elliptic pool, L
b	Minor semi-axis of elliptic pool, L
C	Liquid phase solute concentration (solute mass/liquid volume), M/L^3
C_a	Apparent aqueous phase solute concentration in the presence of doc, M/L^3
C_b	Constant background aqueous phase solute concentration, M/L^3
C_s	Aqueous saturation concentration (solubility), M/L^3
C_Y	Covariance function of Y
$C^\star$	Sorbed solute concentration onto the solid matrix (solute mass/solids mass)
$C^\star_{doc}$	Solute concentration sorbed onto doc (solute mass/liquid volume), M/L^3
$C^{\star\star}_{doc}$	Solute humic concentration sorbed onto the solid matrix (solute mass/solids mass)
D	Molecular diffusion coefficient, L^2/t
D_e	Effective molecular diffusion coefficient, equal to $D/\tau^\star$, L^2/t
D_x	Longitudinal hydrodynamic dispersion coefficients, L^2/t
D_y	Lateral hydrodynamic dispersion coefficients, L^2/t
D_z	Vertical hydrodynamic dispersion coefficient, L^2/t
$erf[\eta]$	Error function, equal to $(2/\pi^{1/2}) \int_0^\eta e^{-\zeta^2} d\zeta$
f	Arbitrary function
h	Total head potential, L
H	Concentration of humic substances in the aqueous phase expressed as doc, M/L^3
H_0	Source concentration of humic substances expressed as doc, M/L^3
k	Local mass transfer coefficient, defined in Eq. (3), L/t
$\hat{k}$	Time invariant local mass transfer coefficient, defined in Eq. (4), L/t
$\overline{k}$	Time dependent average mass transfer coefficient, defined in Eq. (5), L/t
$k^\star$	Time invariant average mass transfer coefficient, defined in Eq. (6), L/t
k_e	Effective local mass transfer coefficient, defined in Eq. (46), L/t
$\overline{k}_e$	average effective mass transfer coefficient, defined in Eq. (47), L/t
K	Hydraulic conductivity, L/t
K_d	Solute partition coefficient between the solid matrix and the aqueous phase, L^3/M
K_{doc}	Solute partition coefficient between the doc and aqueous phase, L^3/M
K_h	Humic substance partition coefficient between solid matrix and aqueous phase, L^3/M
ℓ_c	Characteristic length, L
ℓ_x	Pool dimension in x direction, L
ℓ_{x_o}	x Cartesian coordinate of the origin of a rectangular pool or the center of an elliptic/circular pool, L

ℓ_y	Pool dimension in y direction, L
ℓ_{y_o}	y Cartesian coordinate of the origin of a rectangular pool or the center of an elliptic/circular pool, L
L_h	Humic substance source height, L
m_1, m_2	Defined in Eqs. (22) and (23), respectively
n_1, n_2	Defined in Eqs. (24) and (25), respectively
N	Number of different realizations of the hydraulic conductivity field
Pe_x	Local Peclet number in the longitudinal direction
$Pe_x^\star$	Average Peclet number in the longitudinal direction
Pe_y	Local Peclet number in the transverse direction
$Pe_y^\star$	Average Peclet number in the transverse direction
r	Radius of circular pool, L
r_x	Separation distance in the longitudinal direction of two K measurements, L
r_z	Separation distance in the vertical direction of two K measurements, L
r	Vector with magnitude equal to the separation distance of two K measurements
R	Dimensionless retardation factor
R_s	Dimensionless retardation factor of a solute in the presence of humics, defined in Eq. (45)
R_h	Dimensionless retardation factor of the humic substances, defined in Eq. (50)
R_{sh}	Dimensionless retardation factor of the solute humic substances, defined in Eq. (56)
$R_{(e)}$	Domain defined by an elliptic NAPL-water interfacial area
$R_{(r)}$	Domain defined by a rectangular NAPL-water interfacial area
Sh	Local Sherwood number
$Sh^\star$	Average Sherwood number
t	Time, t
U_x	Interstitial fluid velocity in the longitudinal direction, L/t
U_z	Interstitial fluid velocity in the vertical direction, L/t
U	Interstitial velocity vector
v	Defined in Eq. (26)
x	Spatial coordinate, L
y	Spatial coordinate, L
Y	Logtransformed hydraulic conductivity, equal to $ln\ K$
$\bar{Y}$	Mean logtransformed hydraulic conductivity
z	Spatial coordinate, L
α_L	Longitudinal dispersivity, L
α_T	Transverse dispersivity, L
$\beta_1, \beta_2, \beta_3$	Empirical coefficients
$\gamma_1, \gamma_2, \gamma_3$	Empirical coefficients
ε	Eccentricity, defined in Eq. (27)
ζ_x	Correlation length scale in the longitudinal direction, L
ζ_z	Correlation length scale in the vertical direction, L
θ	Porosity (liquid volume/aquifer volume), L^3/L^3
κ_1, κ_2	Defined in Eqs. (16) and (17), respectively
λ	First-order decay coefficient, t^{-1}
μ	Dummy integration variable
μ_1, μ_2	Defined in Eqs. (20) and (21), respectively
ξ_1, ξ_2	Defined in Eqs. (18) and (19), respectively
ρ_b	Bulk density of the solid matrix, M/L^3
σ_Y^2	Variance of $\ln K$
τ	Dummy integration variable

τ^*	Tortuosity coefficient (≥1)
ADI	Alternating direction implicit
doc	Dissolved organic carbon
DNAPL	Dense nonaqueous phase liquid
NAPL	Nonaqueous phase liquid
PCE	Perchloroethylene
TCE	Trichloroethylene
1,1,2-TCA	1,1,2-Trichloroethane

1 Introduction

The contamination of natural subsurface systems by nonaqueous phase liquids (NAPLs), has captured the attention of many environmental engineers and scientists. Most of the NAPLs are organic solvents and petroleum hydrocarbons originating from leaking underground storage tanks, ruptured pipelines, surface spills, hazardous waste landfills, disposal sites, and leachates from recycled wastes. When an NAPL spill infiltrates the subsurface environment through the vadose zone, a portion of it may be trapped and immobilized within the unsaturated porous formation in the form of blobs or ganglia, which are no longer connected to the main body of the nonaqueous phase liquid. Upon reaching the water table, dense nonaqueous phase liquids (DNAPLs) with densities heavier than that of water (sinkers, e.g., organic leachates from recycled hazardous solid wastes), given that the pressure head at the capillary fringe is sufficiently large, continue to migrate downward leaving behind trapped ganglia until they encounter an impermeable layer, where a flat source zone or pool starts to form [1–3]. On the other hand, NAPLs with densities lower than that of water (floaters, e.g., petroleum products) as soon as they approach the saturated region, spread laterally and float on the water table in the form of a pool [4].

As groundwater flows past trapped ganglia or NAPL pools, a fraction of the NAPL dissolves in the aqueous phase and a plume of dissolved hydrocarbons is created as illustrated in Fig. 1. The dissolved NAPL concentrations may reach saturation or near saturation levels [5]. It should be noted that the dissolution of NAPL pools in porous media is fundamentally different than that of residual blobs. NAPL pools have limited contact areas with respect to groundwater. If the same amount of a NAPL is present as ganglia and as pool, ganglia dissolution is expected to proceed at a faster rate, because of the larger surface area available for interphase mass transfer [6]. Therefore, NAPL pools often lead to longlasting sources of groundwater contamination.

The concentration of a dissolved NAPL in groundwater is governed mainly by interface mass-transfer processes that often are slow and rate-limited [7, 8]. There is a relatively large body of available literature on the migration of NAPLs and dissolution of residual blobs [6, 9–22], and pools [5, 23–34]. Furthermore, empirical correlations useful for convenient estimation of NAPL dissolution

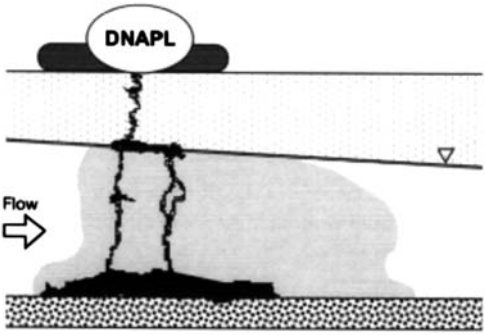

Fig. 1 Schematic illustration of slightly soluble in water dense nonaqueous phase liquid migration in the subsurface and plume formation of dissolved hydrocarbons

rates, expressed in terms of non dimensional parameters, for well defined residual blobs are available in the literature [11, 15, 35]. These correlations relate the Reynolds number and NAPL volumetric fraction to the dimensionless mass transfer rate coefficient (Sherwood number), and differ mainly in the number and type of dimensionless system properties accounted for. The existing correlations indicate that dissolution rates for residual NAPLs in one-dimensional soil columns are highly dependent on blob shape and size, interstitial velocity, and/or length of soil zone exposed to residual NAPLs [8, 15].

Mathematical models for mass transfer at the NAPL-water interface often adopt the assumption that thermodynamic equilibrium is instantaneously approached when mass transfer rates at the NAPL-water interface are much faster than the advective-dispersive transport of the dissolved NAPLs away from the interface [28, 36]. Therefore, the solubility concentration is often employed as an appropriate concentration boundary condition specified at the interface. Several experimental column and field studies at typical groundwater velocities in homogeneous porous media justified the above equilibrium assumption for residual NAPL dissolution [9, 37–39].

2 Mass Flux at the NAPL-Water Interface

As a NAPL pool dissolves into the interstitial fluid of a water saturated porous formation, a concentration boundary layer is assumed to be developed above the NAPL-water interface. Assuming that the thickness of the pool is insignificant relative to the thickness of the aquifer, the mass transfer from the NAPL-water interface into the aqueous interstitial fluid within a three-dimensional, saturated porous formation is described by the following relationship [40]:

$$-D_e \left.\frac{\partial C(t,x,y,z)}{\partial z}\right|_{z\to 0} = k(t,x,y)\left[C_s - C(t,x,y,\infty)\right] \tag{1}$$

where $C(t, x, y, z)$ is the aqueous phase solute concentration; x, y, z are the spatial coordinates in the longitudinal, transverse and vertical (perpendicular to the interface) directions, respectively; t is time; $D_e=D/\tau^*$ is the effective molecular diffusion coefficient (where D is the molecular diffusion coefficient, and $\tau^*\geq 1$ is the tortuosity coefficient); $k(t, x, y)$ is the local mass transfer coefficient dependent on time and location at the NAPL-water interface; and C_s is the aqueous saturation (solubility) concentration of the NAPL at the interface. Conventionally, any location above the concentration boundary layer is considered as $z\rightarrow\infty$. For the case where the background concentration is constant with respect to time and space, for notational convenience, $C(t, x, y, \infty)$ is replaced by C_b, the constant background aqueous phase concentration. It should be noted that in all of the cases considered in this chapter the free stream concentration is assumed to be zero ($C_b=0$). The left-hand side term in Eq. (1) represents a diffusive flux given by Fick's law, whereas the right-hand side represents a convective mass transfer flux. The mass transfer relationship given by Eq. (1) implies that the dissolution at the NAPL-water interface is fast. Therefore, the aqueous phase solute concentration is limited only by mass transfer. The concentration along the interface is assumed constant and equal to the saturation concentration,

$$C(t, x, y, 0) = C_s \tag{2}$$

The development of a concentration boundary layer at steady-state uniform flow conditions for two different constant background liquid phase concentrations is shown in Fig. 2. The NAPL-water interface is indicated by the x-axis, whereas the concentration within the boundary layer is shown with arrows. Traditionally, arrows are reserved for the representation of vectors; however, arrows are employed in Fig. 2 for convenient sketching of the magnitude of the scalar concentration. The first case (Fig. 2a) illustrates the situation where the background liquid phase concentration is zero and the concentration within the boundary layer decreases from saturation concentration at the NAPL-water interface to zero concentration in the bulk interstitial liquid. The second case (Fig. 2b) represents the situation where the background concentration is constant, but nonzero, and the concentration within the boundary layer varies from the solubility limit at the interface to a finite constant concentration in the bulk interstitial fluid. The thickness of the boundary layer depends mainly on the hydrodynamics and dispersion properties of the system, and is defined as the value of z for which $[C(t, x, y, 0)-C(t, x, y, z)]/[C(t, x, y, 0)-C(t, x, y, \infty)]=0.99$ [41]. Examination of Fig. 2 indicates that a thin boundary layer corresponds to steeper concentration gradients. It should be noted, however, that the greater the concentration gradient the greater the mass transfer of the dissolved component. Therefore, the local mass transfer coefficient decreases with distance from the front end of the NAPL pool and has a maximum value at the leading or upstream edge. The local mass transfer coefficient is not only spatially but temporally dependent during the initial period of formation of the boundary layer. At steady-state physicochemical and hydrodynamic conditions the local mass transfer coefficient is independent of time.

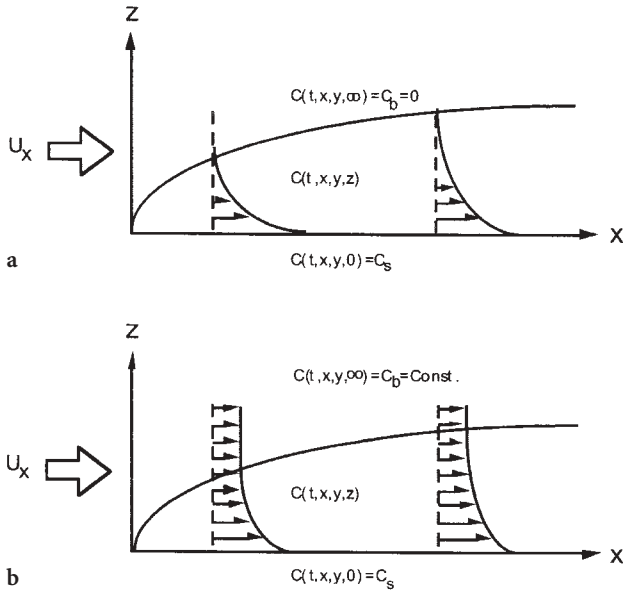

Fig. 2a, b Development of a concentration boundary layer along the NAPL-water interface in uniform interstitial flow for: **a** zero bulk aqueous phase (background) concentration; **b** constant nonzero background concentration (adopted from Chrysikopoulos and Lee [30])

In view of Eq. (1), the time and space dependent local mass transfer coefficient is given by

$$k(t, x, y) = -\frac{D_e}{C_s}\frac{\partial C(t, x, y, z)}{\partial z}\bigg|_{z \to 0} \tag{3}$$

At the relatively rare case where steady-state physicochemical and hydrodynamic conditions exist, the local mass transfer coefficient is independent of time,

$$\hat{k}(x, y) = -\frac{D_e}{C_s}\frac{\partial C(x, y, z)}{\partial z}\bigg|_{z \to 0} \tag{4}$$

It should be noted that the local mass transfer coefficient can only be obtained experimentally and is case specific. An analytical relationship for the local mass transfer rate coefficient can be obtained if a mathematical expression describing the gradient of the dissolved concentration at the NAPL-water interface is known. Unfortunately, the local mass transfer coefficient usually is not an easy parameter to determine with precision. Thus, in mathematical modeling of contaminant transport originating from NAPL pool dissolution, $k(t, x, y)$ is often replaced by the average mass transfer coefficient, $\bar{k}(t)$, applicable to the entire pool, expressed as [41]

$$\bar{k}(t) = \frac{1}{A}\int_A k(t, x, y)\, \mathrm{d}^2\mathbf{A} \tag{5}$$

where A is the surface area of the NAPL pool, and $d^2\mathbf{A}$ is a differential surface area. Furthermore, at steady state conditions $k(t, x, y)$ is replaced by the corresponding time invariant, average mass transfer coefficient, k^*, applicable to the entire pool, expressed as [30]

$$k^* = \frac{1}{A}\int_A \hat{k}(x, y)\ d^2\mathbf{A} \tag{6}$$

3 Analytical Models for NAPL Pool Dissolution and Contaminant Transport in Porous Media

The transient contaminant transport from a dissolving DNAPL pool in a water saturated, three-dimensional, homogeneous porous medium under steady-state uniform flow, assuming that the dissolved organic sorption is linear and instantaneous, is governed by the following partial differential equation:

$$R\frac{\partial C(t, x, y, z)}{\partial t} = D_x\frac{\partial^2 C(t, x, y, z)}{\partial x^2} + D_y\frac{\partial^2 C(t, x, y, z)}{\partial y^2} + D_z\frac{\partial^2 C(t, x, y, z)}{\partial z^2} - U_x\frac{\partial C(t, x, y, z)}{\partial x} - \lambda RC(t, x, y, z) \tag{7}$$

where U_x is the average unidirectional interstitial fluid velocity; D_x, D_y, D_z are the longitudinal, transverse, and vertical hydrodynamic dispersion coefficients, respectively, defined as [42]

$$D_x = \alpha_L U_x + D_e \tag{8a}$$

$$D_y = \alpha_T U_x + D_e \tag{8b}$$

$$D_z = \alpha_T U_x + D_e \tag{8c}$$

where α_L and α_T are the longitudinal and transverse dispersivities, respectively; R is the dimensionless retardation factor accounting for the effects of sorption, representing the ratio of the average interstitial fluid velocity to the propagation velocity of the solute [43], and for linear, instantaneous sorption is given by

$$R = 1 + \frac{\rho_b K_d}{\theta} \tag{9}$$

(where K_d is the partition or distribution coefficient; ρ_b is the bulk density of the solid matrix; and θ is the porosity of the porous medium); and λ is a first-order decay constant. It should be noted that the decay term λRC in the governing Eq. (7) indicates that the total concentration (aqueous plus sorbed solute mass) disappears due to possible decay or biological/chemical degradation.

3.1 Rectangular Pool

For a DNAPL pool with rectangular geometry as shown in Fig. 3a, assuming that NAPL pool dissolution is described by Eq. (1), the appropriate initial and boundary conditions are

$$C(0, x, y, z) = 0 \tag{10}$$

$$C(t, \pm\infty, y, z) = 0 \tag{11}$$

$$C(t, x \pm \infty, z) = 0 \tag{12}$$

$$D_e \frac{\partial C(t, x, y, z)}{\partial z} = \begin{cases} -k(t, x, y)\, C_s & \ell_{x_o} < x < \ell_{x_o} + \ell_x, \\ & \ell_{y_o} < y < \ell_{y_o} + \ell_y, \\ 0 & \end{cases} \tag{13}$$

Otherwise,

$$C(t, x, y, \infty) = 0 \tag{14}$$

where ℓ_{x_o}, ℓ_{y_o} indicate the x, y Cartesian coordinates of the pool origin, respectively, and ℓ_x, ℓ_y are the pool dimensions in x, y directions, respectively. The analytical solution to the governing partial differential Eq. (7) subject to conditions given by Eqs. (10)–(14) for the special case where $k(t, x, y)=k^*$ has been derived by Chrysikopoulos [40] as follows:

$$C(t, x, y, z) = \frac{C_s k^*}{4D_e} \int_0^t \left(\frac{D_z}{R\pi\tau}\right)^{1/2} \exp\left[-\lambda\tau - \frac{Rz^2}{4D_z\tau}\right] \left(\operatorname{erf}[\kappa_1] - \operatorname{erf}[\kappa_2]\right) \left(\operatorname{erf}[\xi_1] - \operatorname{erf}[\xi_2]\right) d\tau \tag{15}$$

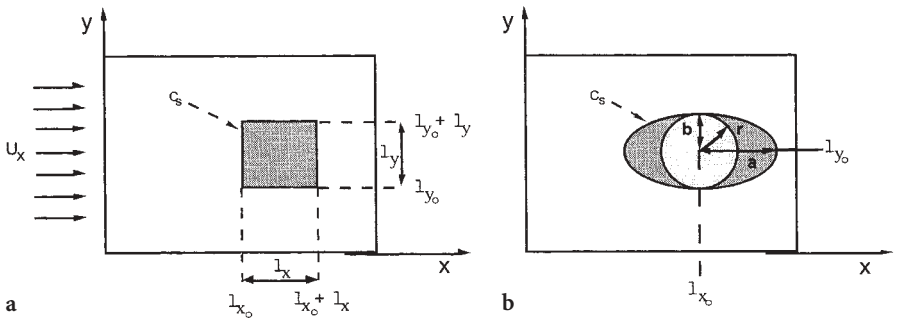

Fig. 3a, b Plan view of a denser than water: **a** rectangular NAPL pool with dimensions $\ell_x \times \ell_y$; **b** elliptic NAPL pool with origin at $x = \ell_{x_o}, y = \ell_{y_o}$ having major semi-axis a and minor semi-axis b. For the special case where $a=b=r$ the elliptic pool becomes a circular pool with radius r

where

$$\kappa_1 = \left(x - \ell_{x_o} - \frac{U_x\tau}{R}\right)\left(\frac{R}{4D_x\tau}\right)^{1/2} \tag{16}$$

$$\kappa_2 = \left(x - \ell_{x_o} - \ell_x - \frac{U_x\tau}{R}\right)\left(\frac{R}{4D_x\tau}\right)^{1/2} \tag{17}$$

$$\xi_1 = (y - \ell_{y_o})\left(\frac{R}{4D_y\tau}\right)^{1/2} \tag{18}$$

$$\xi_2 = (y - \ell_{y_o} - \ell_y)\left(\frac{R}{4D_y\tau}\right)^{1/2} \tag{19}$$

$erf[\ ]$ is the error funktion defined as $erf[\eta] = (2/\pi^{1/2})\int_0^\eta e^{-\zeta^2}\,d\zeta$; and τ is a dummy integration variable. Note that in view of Eq. (1) it is evident that the analytical solution given by Eq. (15) can also be employed for cases of finite but constant free stream concentration (C_b=const.≠0) by replacing C_s by C_s–C_b.

3.2 Elliptic/Circular Pool

For a DNAPL pool with elliptic geometry as shown in Fig. 3b, assuming that NAPL pool dissolution is described by Eq. (1), the appropriate initial and boundary conditions are given by Eqs. (10)–(12), (14) and

$$D_e\frac{\partial C(t,x,y,0)}{\partial z} = \begin{cases} -k(t,x,y)\,C_s \sim \dfrac{(x-\ell_{x_o})^2}{a^2} + \dfrac{(y-\ell_{y_o})^2}{b^2} \le 1 \\ 0 \qquad\qquad\qquad\qquad\qquad\qquad \text{otherwise} \end{cases} \tag{20}$$

where a and b are the major and minor semi-axes of the elliptic pool, respectively; and ℓ_{x_o} and ℓ_{y_o} indicate the x and y Cartesian coordinates of the pool origin, respectively.

The analytical solution to the governing partial differential Eq. (7) subject to conditions given by Eqs. (10)–(12), (14), and (20) for the special case where $k(t,x,y)=k^\star$ has been derived by Chrysikopoulos [40] as follows:

$$C(t,x,y,z) = \frac{C_s k^\star}{4D_e}\int_0^t\int_{m_1}^{m_2}\left(\frac{D_z}{R\tau}\right)^{1/2}\exp\left[-\lambda\tau - \frac{Rz^2}{4D_z\tau}\right] \times \exp[-\mu^2]\,(\mathrm{erf}[-n_2] - \mathrm{erf}[n_1])\,d\mu\,d\tau, \tag{21}$$

where

$$m_1 = (y - \ell_{y_o} + b)\left(\frac{R}{4D_y\tau}\right)^{1/2} \tag{22}$$

$$m_2 = (y - \ell_{y_o} - b)\left(\frac{R}{4D_y\tau}\right)^{1/2} \tag{23}$$

$$n_1 = \left[x - \frac{U_x\tau}{R} - \ell_{x_o} + \left\{\left[1 - \frac{(v - \ell_{y_o})^2}{b^2}\right]a^2\right\}^{1/2}\right]\left(\frac{R}{4D_x\tau}\right)^{1/2} \tag{24}$$

$$n_2 = \left[x - \frac{U_x\tau}{R} - \ell_{x_o} - \left\{\left[1 - \frac{(v - \ell_{y_o})^2}{b^2}\right]a^2\right\}^{1/2}\right]\left(\frac{R}{4D_x\tau}\right)^{1/2} \tag{25}$$

$$v = y - \mu\left(\frac{4D_y\tau}{R}\right)^{1/2} \tag{26}$$

μ and τ are dummy integration variables. Note that in view of Eq. (1) it is evident that the analytical solution given by Eq. (21) can also be employed for cases of finite but constant free stream concentration (C_b=const.≠0) by replacing C_s by C_s–C_b.

A circular pool with radius r, as shown in Fig. 3b, is equivalent to an elliptic pool when a=b=r. Because the circular pool geometry is a special case of an elliptic pool, the appropriate solution to the case of a circular pool can be obtained directly from Eq. (21) by substituting a=b=r.

3.3 Model Simulations

The analytical solution for a rectangular pool, Eq. (15), is employed to simulate dissolved concentrations originating from the NAPL pool along the rectangular-pool centerline in the downstream direction at z=0.04 m from three NAPL pool sources of equal surface area with dimensions $\ell_x \times \ell_y$ of 1×9 m^2, 3×3 m^2, and 9×1 m^2, respectively. The results are presented in Fig. 4a and clearly indicate that the source structure and orientation control the concentration level of the dissolved NAPL. The longer the pool in the direction of flow, the higher the dissolved peak concentration in the interstitial fluid. However, the wider the pool perpendicular to the direction of flow, the larger the immediate downstream area covered by the dissolved contaminant.

The analytical solution for an elliptic pool, Eq. (21), is employed to investigate the effect of eccentricity, ε, of an elliptic NAPL pool on dissolved contaminant concentration. The model simulations are presented in Fig. 4b. It should be noted that the eccentricity of an elliptic pool is defined as

$$\varepsilon = \left[1 - \left(\frac{b}{a}\right)^2\right]^{1/2} \tag{27}$$

When ε=0, then a=b and the elliptic pool becomes circular. The closer ε is to one, the more elongated the elliptic pool. Figure 4b shows that the dissolved conta-

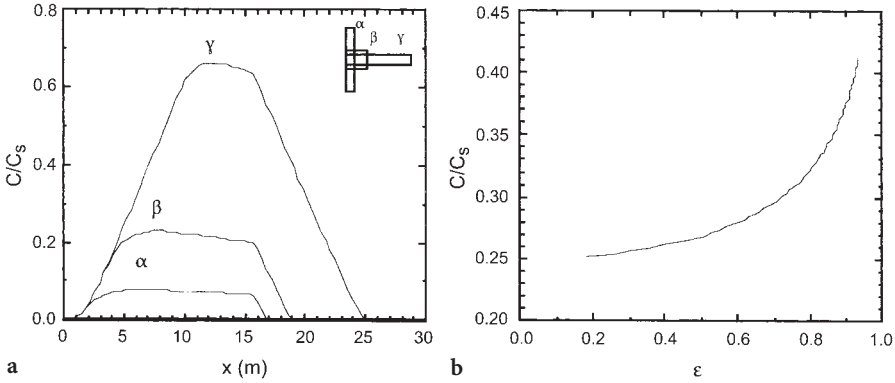

Fig. 4a, b Distribution of normalized aqueous phase NAPL concentration as a function of downstream distance for pools of equal surface area and dimensions $\ell_x \times \ell_y$ (α) 1×9 m^2, (β) 3×3 m^2, and (γ) 9×1 m^2, (here ℓ_{x_o}=0 m, ℓ_{y_o}=0, 3, 4 m for cases α, β, and γ, respectively, y=4.5 m, z=0.04 m); (b) Normalized aqueous phase NAPL concentration predicted at a location with coordinates (x, y, z)=(10, 5, 0.04 m) as a function of eccentricity of an elliptic pool (here $\ell_{x_o}=\ell_{y_o}$=5 m)

minant concentration at (x, y, z)=(10, 5, 0.04 m) within a three-dimensional homogeneous porous formation is increasing with increasing ε. Certainly, the result of Fig. 4b is in perfect agreement with that of Fig. 4a.

4
NAPL Pool Dissolution in Heterogeneous Formations

The effects of aquifer anisotropy and heterogeneity on NAPL pool dissolution and associated average mass transfer coefficient have been examined by Vogler and Chrysikopoulos [44]. A two-dimensional numerical model was developed to determine the effect of aquifer anisotropy on the average mass transfer coefficient of a 1,1,2-trichloroethane (1,1,2-TCA) DNAPL pool formed on bedrock in a statistically anisotropic confined aquifer. Statistical anisotropy in the aquifer was introduced by representing the spatially variable hydraulic conductivity as a log-normally distributed random field described by an anisotropic exponential covariance function.

4.1
Two-Dimensional Numerical Model

The transport of a sorbing contaminant in two-dimensional, heterogeneous, saturated porous media, resulting from the dissolution of a single component NAPL pool, as illustrated in Fig. 5, is described by the following partial differential equation [44]:

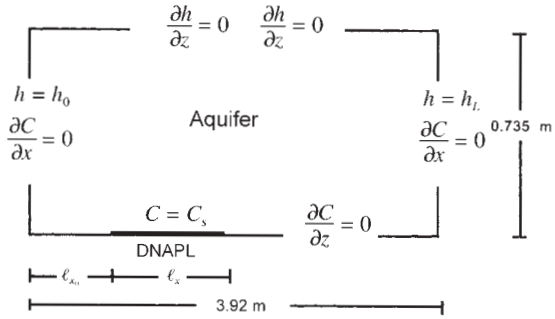

Fig. 5 Schematic illustration of the physical system examined, showing the DNAPL pool location and the appropriate boundary conditions employed in the numerical model

$$R\frac{\partial C(t,x,z)}{\partial t} = \frac{\partial}{\partial x}\left[D_x(x,z)\frac{\partial C(t,x,z)}{\partial x}\right] + \frac{\partial}{\partial z}\left[D_z(x,z)\frac{\partial C(t,x,z)}{\partial z}\right] - \frac{\partial}{\partial x}\left[U_x(x,z)\,C(t,x,z)\right] - \frac{\partial}{\partial z}\left[U_z(x,z)\,C(t,x,z)\right], \tag{28}$$

where U_z is the vertical interstitial fluid velocity. It was assumed that the NAPL phase is immobile, and aquifer anisotropy is governed by the variability in the hydraulic conductivity field. The two-dimensional hydraulic conductivity field was generated stochastically with the computer program SPRT2D [45]. Furthermore, it was assumed that the hydraulic conductivity follows a log-normal distribution and the log-transformed hydraulic conductivity, Y, varies spatially according to the following anisotropic exponential covariance function [27, 46–48]:

$$C_Y(\mathbf{r}) = \sigma_Y^2 \exp\left[-\left(\frac{r_x^2}{\zeta_x^2} + \frac{r_x^2}{\zeta_z^2}\right)^{1/2}\right] \tag{29}$$

where $\mathbf{r}=(r_x, r_z)^T$ is a two-dimensional vector whose magnitude is the separation distance of two hydraulic conductivity measurements; ζ_x and ζ_z are the correlation length scales in the x and z directions, respectively; and σ_Y^2 is the variance of the log transformed hydraulic conductivity defined as

$$Y = \ln K \tag{30}$$

where K is the hydraulic conductivity. It should be noted that the stochastic realizations of $K(x, z)$ are locally independent of direction, and that anisotropy is introduced globally by the overall spatial variability of the hydraulic conductivity field [49].

For each hydraulic conductivity field generated, the associated variable hydraulic head field and groundwater velocity field were determined. Each variable hydraulic head field was evaluated numerically by solving the following steady state two-dimensional groundwater flow equation for a heterogeneous confined aquifer [50]:

$$\frac{\partial}{\partial x}\left[K(x,z)\frac{\partial h(x,z)}{\partial x}\right]+\frac{\partial}{\partial z}\left[K(x,z)\frac{\partial h(x,z)}{\partial z}\right]=0 \tag{31}$$

where $h(x, z)$ is the hydraulic head, that is equal to total head potential. The interstitial groundwater flow velocities, used in the governing transport Eq. (28), were determined using the hydraulic head distribution obtained by solving Eq. (31) in conjunction with the following equations:

$$U_x(x,z)=\frac{K(x,z)}{\theta}\frac{\partial h(x,z)}{\partial x} \tag{32}$$

$$U_x(x,z)=\frac{K(x,z)}{\theta}\frac{\partial h(x,z)}{\partial z} \tag{33}$$

where θ is the effective porosity of the porous medium. The porosity was assumed constant even though the hydraulic conductivity field is variable [51, 52]. The spatially variable hydrodynamic dispersion coefficients were calculated using the following relationships [50]:

$$D_x(x,z)=\frac{\alpha_T U_z^2(x,z)+\alpha_T U_x^2(x,z)}{|\mathbf{U}|}+D_e \tag{34a}$$

$$D_z(x,z)=\frac{\alpha_T U_x^2(x,z)+\alpha_T U_z^2(x,z)}{|\mathbf{U}|}+D_e \tag{34b}$$

where

$$|\mathbf{U}|=[U_x^2(x,z)+U_z^2(x,z)]^{1/2} \tag{35}$$

is the magnitude of the interstitial velocity vector. Local time dependent mass transfer coefficient values along the length of the NAPL pool were determined by modifying Eq. (5) so that $\bar{k}(t)$ can efficiently be evaluated numerically as follows:

$$\bar{k}(t)=\frac{1}{\ell_x N}\sum_{i=1}^{N}\int_{\ell_{x_o}}^{\ell_{x_o}+\ell_x} k_i(t,x)\,dx \tag{36}$$

where N is the number of different log-normally distributed hydraulic conductivity field realizations examined.

The contaminant transport model, Eq. (28), was solved using the backwards in time alternating direction implicit (ADI) finite difference scheme subject to a zero dispersive flux boundary condition applied to all outer boundaries of the numerical domain with the exception of the NAPL-water interface where concentrations were kept constant at the 1,1,2-TCA solubility limit C_s. The groundwater model, Eq. (31), was solved using an implicit finite difference scheme subject to constant head boundaries on the left and right of the numerical domain, and no-flux boundary conditions for the top and bottom boundaries, corresponding to the confining layer and impermeable bedrock, respectively, as

schematically illustrated in Fig. 5. For each realization of the hydraulic conductivity field, local mass transfer coefficients were determined at each node at the NAPL-water interface from [24]:

$$D_e \frac{\partial C(t, x, 0)}{\partial z} = -k(t, x)\, C_s \qquad \ell_{x_o} < x < \ell_{x_o} + \ell_x \tag{37}$$

by using the second-order accurate one-sided approximation of the concentration gradient above the NAPL pool [53]. The local mass transfer coefficients were averaged over the length of the NAPL pool and the average mass transfer coefficient was determined from Eq. (36) by averaging the results from the various realizations of the hydraulic conductivity field.

4.2 Numerical Model Simulations

The numerical model was employed to obtain aqueous phase concentrations originating from the dissolution of a 1,1,2-TCA pool in a heterogeneous, isotropic formation for two different variances of the log-transformed hydraulic conductivity distribution. The generated contours are presented in Fig. 6. Clearly, the results presented in Fig. 6 indicate that with increasing σ_Y^2 the heterogeneity of the porous medium is increased, the spreading of the dissolved plume is increased in the vertical direction, and consequently, the concentration gradients at the pool-water interface are reduced leading to $\bar{k}$ reduction.

Numerically evaluated average mass transfer coefficients, $\bar{k}$, based on the average of 200 different realizations of the log-normal hydraulic conductivity, as a function of ζ_z/ζ_x for several variances of $Y=\ln K$ (σ_Y^2 =0.1, 0.2, 0.3, 0.4, and 0.5) for a hydraulic gradient of $\partial h/\partial x$=0.01 and mean log-transformed hydraulic conductivity of $\bar{Y}$=0.8 are shown in Fig. 7a. The results indicate that for increasing ζ_z/ζ_x there is a significant increase in $\bar{k}$. Low values of the anisotropy

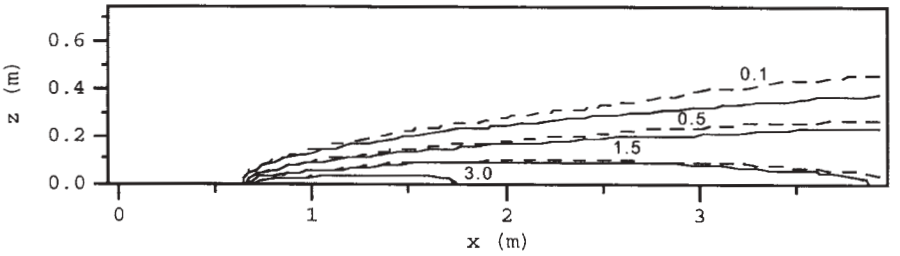

Fig. 6 Comparison between aqueous phase 1,1,2-TCA concentration contours originating from a 1,1,2-TCA pool for σ_Y^2=0.5 (*dashed line*) and 0.1 (*solid line*) (here C_s=4.5 g/l, D_e=2.33 $\times 10^{-6}$ m^2/h, ℓ_{x_o}=0.64 m, ℓ_x=0.72 m, R=1.63, t=5,000 h, $\bar{Y}$=0.8, $\partial h/\partial x$=0.01, α_L=3.3$\times 10^{-2}$ m, α_T=3.3$\times 10^{-3}$ m, ζ_x=0.5 m, ζ_z=0.5 m, θ=0.3) (adopted from Vogler and Chrysikopoulos [44])

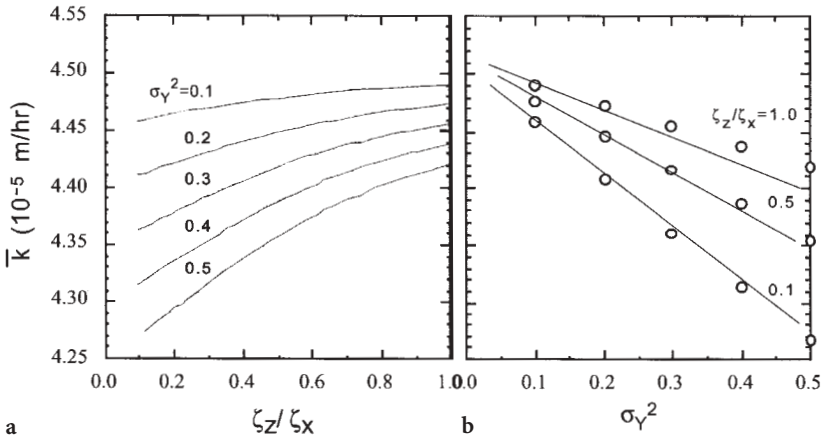

Fig. 7a, b Average mass transfer coefficient as a function of: **a** aquifer anisotropy ratio for several variances of the log-transformed hydraulic conductivity distribution; **b** variance of the log-transformed hydraulic conductivity distribution where *open circles* represent numerically generated data and *solid lines* represent linear fits. All model parameter values are identical with those used in Fig. 6

ratio ζ_z/ζ_x may represent the presence of thin lenticular layers of varying hydraulic conductivity which are observed in some sedimentary rocks [54]. Consequently, for low ζ_z/ζ_x ratios, transverse dispersion is significant causing more vertical spreading of the dissolved 1,1,2-TCA concentration plume which in turn leads to a thicker concentration boundary layer, smaller concentration gradients at the pool water interface, and smaller $\bar{k}$ values. Increasing ζ_z/ζ_x, the hydraulic conductivity becomes progressively more statistically similar in the vertical direction. For high ζ_z/ζ_x ratios the aqueous phase 1,1,2-TCA concentration boundary layer is thinner because vertical dispersion is reduced across statistically similar lenticular layers yielding steeper concentration gradients at the pool-water interface and greater $\bar{k}$ values.

Numerically evaluated $\bar{k}$ values, based on the average of 200 different realizations of the lognormal hydraulic conductivity, as a function of σ_Y^2 for several anisotropy ratios (ζ_z/ζ_x=0.1, 0.5, and 1.0) for a hydraulic gradient of $\partial h/\partial x$=0.01 and mean log-transformed hydraulic conductivity of $\bar{Y}$=0.8 are shown in Fig. 7b together with the best fitted lines. The results indicate that $\bar{k}$ is inversely proportional to σ_Y^2. Furthermore, in agreement with the results presented in Fig. 7a, it is also evident from Fig. 7b that $\bar{k}$ values increase with increasing ζ_z/ζ_x. However, increasing σ_Y^2 results in increased aquifer heterogeneity with a broader range of K values.

5
NAPL Pool Dissolution in the Presence of Dissolved Humic Substances

Humic substances are the most abundant, polydisperse organic materials in nature. They are formed by oxidation and condensation reactions between polyphenols, polysaccharides, and polyamino acids of plant and microbial origin [55]. Humic substances found in groundwater originate from infiltrating surface water, and from paleo-soils that were buried during geological sedimentation. The ability of humic substances to interact with hydrophobic organic compounds and to enhance hydrophobic organic solubility by a partitioning process is widely recognized [56]. However, the exact solubility enhancement mechanism is not well understood. The capability of dissolved humic substances to increase NAPL pool dissolution rates and enhance contaminant transport in a two-dimensional, homogeneous porous formation has been explored by Tatalovich et al. [57].

A two-dimensional numerical model was developed to describe the transport of dissolved organics originating from nonaqueous phase liquid pool dissolution in saturated porous media in the presence of dissolved humic substances. The model assumes that the dissolved contaminant (NAPL dissolved in the aqueous phase) may sorb onto the solid matrix as well as onto humic substances suspended in the aqueous phase, contaminant-humic particles and humic substances may sorb onto the solid matrix, the dissolved contaminant may undergo first-order decay, and humic substances are introduced into the aquifer from a line source.

5.1
Two-Dimensional Solute-Humic Cotransport Numerical Model

The appropriate mathematical model for solute transport originating from the dissolution of a perchloroethylene (PCE) pool located onto a bedrock within a two-dimensional, homogeneous, water saturated aquifer in the presence of dissolved humic substances, as illustrated in Fig. 8, consists of three coupled transport equations. One equation describing the transport of the solute originating from the dissolving PCE pool in the presence of dissolved humic substances, another equation describing the transport of dissolved humic substances, and the third equation describing the transport of solute-humic particles.

5.1.1
Solute Transport and Effective Mass Transfer

The two-dimensional transient transport of the solute originating from the dissolution of a PCE pool in saturated, homogeneous porous media under uniform interstitial groundwater flow and in the presence of dissolved humic substances is governed by [57]

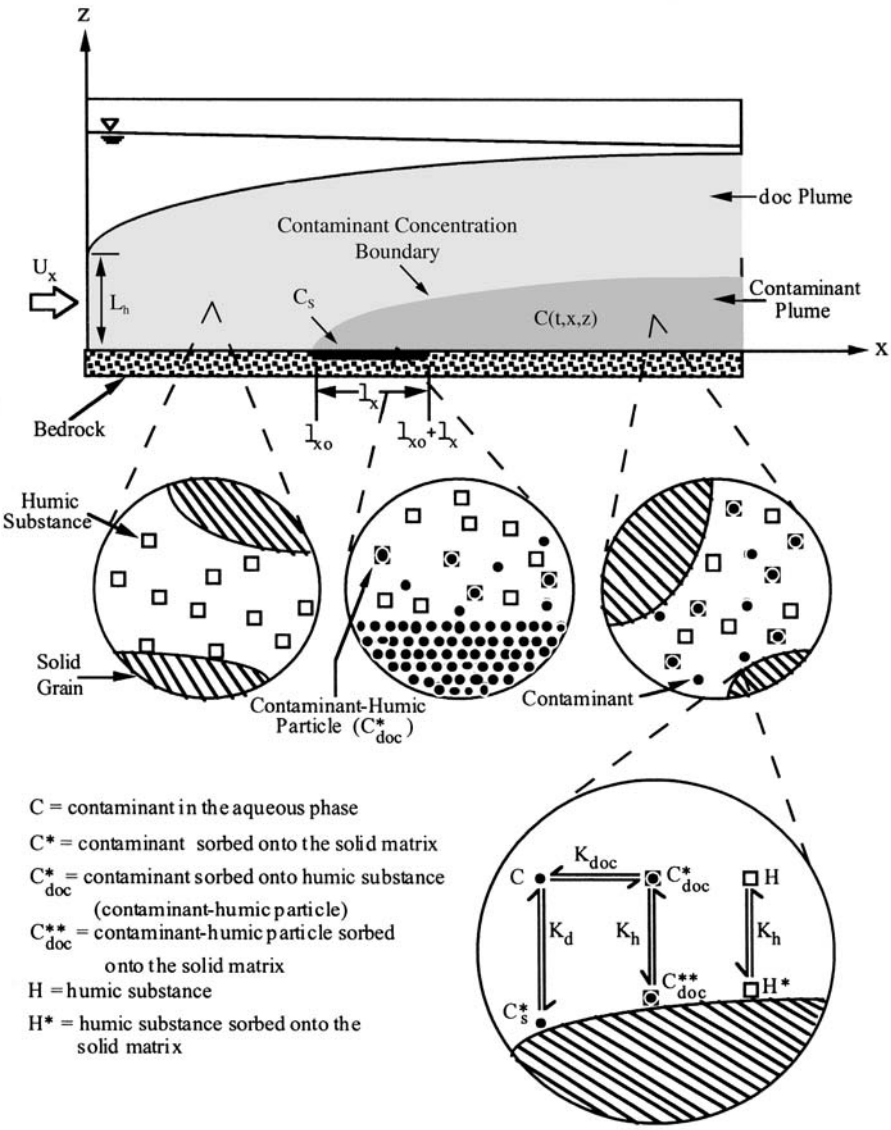

Fig. 8 Schematic diagram of the conceptual model showing the unidirectional velocity U_x, the DNAPL pool with aqueous saturation concentration C_s, the humic substance line source of height L_h, and the modes of interaction between dissolved contaminant, dissolved humic substances, and the solid matrix (adopted from Tatalovich et al. [57])

$$\frac{\partial}{\partial t}\left[R_s(t,x,z)\,C(t,x,z)\right] = D_{x_s}\frac{\partial^2 C(t,x,z)}{\partial x^2} + D_{z_s}\frac{\partial^2 C(t,x,z)}{\partial z^2} - U_x\frac{\partial C(t,x,z)}{\partial x} - \lambda_s R_s(t,x,z)\,C(t,x,z) \tag{38}$$

where the subscript s indicates the solute; and $R_s(t, x, z)$ is the time and space dependent, dimensionless retardation factor of the solute.

Assuming that there is no initial dissolved PCE concentration in the homogeneous, two-dimensional, water saturated formation of infinite dimension along the x direction and semi-infinite dimension along the z direction with an impervious boundary at z=0, as illustrated in Fig. 8, the appropriate initial and boundary conditions are

$$C(0,x,z) = 0 \tag{39}$$

$$\frac{\partial C(t,\pm\infty,z)}{\partial x} = \frac{\partial C(t,x,\infty)}{\partial z} = 0 \tag{40}$$

$$\frac{\partial C(t,x,0)}{\partial z} = \begin{cases} \dfrac{\partial C_a(t,x,0)}{\partial z} & \ell_{x_o} \le x \le \ell_{x_o} + \ell_x, \\ 0 \end{cases} \tag{41}$$

otherwise, where $C_a(t, x, z)$ is the apparent (enhanced) aqueous phase solute concentration due to the presence of dissolved organic carbon (doc).

Numerous experimental studies suggest that a linear relationship exists between NAPL solubility and dissolved humic substance concentration [58–63]. Consequently, for a two-dimensional system, the apparent aqueous phase solute concentration at the NAPL-water interface can be expressed as [56]

$$C_a(t,x,z) = C_s[1 + K_{doc}\,H(t,x,0)] \tag{42}$$

where $H(t, x, z)$ is the dissolved organic carbon concentration attributable to humic substances; and K_{doc} is the solute partition coefficient between humic substances and the aqueous phase (based on the doc concentration). It should be noted that for $z \neq 0$ the aqueous solubility, C_s, present in Eq. (42) should be replaced by the aqueous phase solute concentration, $C(t, x, z)$.

Assuming that the process of solute sorption onto the solid matrix can be described by the following linear equilibrium relationship:

$$C^{\star}(t,x,0) = K_d\,C(t,x,z) \tag{43}$$

where $C^*(t, x, z)$ is the solute concentration sorbed onto the solid matrix, and that, in view of Eq. (42), the process of solute sorption onto dissolved humic substances is described by the following expression:

$$C^{\star}_{\mathrm{doc}}(t,x,z) = K_{doc}\,C(t,x,z)\,H(t,x,z) \tag{44}$$

where $C^{\star}_{\mathrm{doc}}(t, x, z)$ is the solute concentration sorbed onto dissolved organic carbon; consequently, the time and space dependent, dimensionless retardation factor of the solute, $R_s(t, x, z)$, is given by

$$R_s(t, x, z) = 1 + \frac{\rho_{\mathrm{b}} K_d}{\theta} + K_{doc} H(t, x, z) \tag{45}$$

Given that the presence of humics enhance the solute solubility, the local mass transfer coefficient, k, defined in Eq. (3) should be modified accordingly. In view of Eq. (42), the appropriate expression for the effective local mass transfer coefficient, $\bar{k}_e(t, x)$, is given by [57]

$$\begin{aligned} k_e(t, x) &= -\frac{D_e}{C_s} \frac{\partial}{\partial z} [C(t, x, 0) + C^{\star}_{\mathrm{doc}}(t, x, 0)] \\ &= -\frac{D_e}{C_s} \frac{\partial C_a(t, x, 0)}{\partial z} \end{aligned} \tag{46}$$

In the absence of dissolved humic substances, the preceding equation reduces to the local mass transfer coefficient defined in Eq. (3). Furthermore, the corresponding average effective mass transfer coefficient, $\bar{k}_e(t)$, applicable to the entire pool, can be expressed as

$$\bar{k}_e(t) = \frac{1}{\ell_x} \int_0^{\ell_x} k_e(t, x)\, \mathrm{d}x \tag{47}$$

5.1.2 Transport of Dissolved Humic Substances

The two-dimensional transient transport of dissolved humic substances in water saturated, homogeneous porous media under uniform interstitial groundwater flow is governed by the following partial differential equation:

$$R_h \frac{\partial H(t, x, z)}{\partial t} = D_{x_h} \frac{\partial^2 H(t, x, z)}{\partial x^2} + D_{z_h} \frac{\partial^2 H(t, x, z)}{\partial z^2} - U_x \frac{\partial H(t, x, z)}{\partial x} \tag{48}$$

where the subscript h indicates the dissolved humic substance; and R_h is the dimensionless retardation factor for humic substances. The governing transport Eq. (48) does not account for decay of humic substances because they are usually stable and persistent in the environment. Note that the dispersion coefficients for the solute-humic substances are differentiated from the dispersion coefficients for the solute because of their differences in molecular size and structure. Sorption of dissolved humic substances onto solids is often described mathematically as a linear equilibrium, Langmuir, or Freundlich process [64–67]. Here it is assumed that the sorption of dissolved humic substances onto the solid matrix is described by the following linear relationship:

$$H^{\star}(t, x, z) = K_h\, H(t, x, z) \tag{49}$$

where $H^{\star}(t, x, z)$ is the dissolved organic carbon concentration sorbed onto the solid matrix; and K_h is the humic substance linear equilibrium partition coefficient between the solid matrix and the aqueous phase. Consequently, the retardation factor, R_h, is given by

$$R_h = 1 + \frac{\rho_b\, K_h}{\theta} \tag{50}$$

Assuming that initially there are no dissolved humic substances in the homogeneous, two-dimensional, water saturated formation considered here, and the humic substances are introduced in the porous medium from a continuous line source of height L_h, located at x=0, y=0, as indicated in Fig. 8, the appropriate initial and boundary conditions are

$$H_0(0, x, z) = 0 \tag{51}$$

$$H(t, 0, z \le L_h) = H_0 \tag{52}$$

$$\frac{\partial H(t, \pm\infty, z)}{\partial x} = \frac{\partial H(t, x, \infty)}{\partial z} = \frac{\partial H(t, x, 0)}{\partial z} = 0 \tag{53}$$

where H_0 is the source concentration of dissolved humic substances expressed as doc.

5.1.3 Transport of Solute-Humic Substances

The two-dimensional, transient transport of solute-humic substances in water saturated, homogeneous porous media under uniform interstitial groundwater is governed by the following partial differential equation:

$$R_{sh}\frac{\partial C^{\star}_{\mathrm{doc}}(t, x, z)}{\partial t} = D_{x_{sh}}\frac{\partial^2 C^{\star}_{\mathrm{doc}}(t, x, z)}{\partial x^2} + D_{z_{sh}}\frac{\partial^2 C^{\star}_{\mathrm{doc}}(t, x, z)}{\partial z^2} - U_x\frac{\partial^2 C^{\star}_{\mathrm{doc}}(t, x, z)}{\partial x} - \lambda_{sh}\, R_{sh}\, C^{\star}_{\mathrm{doc}}(t, x, z) \tag{54}$$

where subscript *sh* indicates the solute-humic substance; and R_{sh} is the dimensionless retardation factor for the dissolved solute-humic substances. Assuming that the sorption of dissolved solute-humic substances onto the solid matrix is described by the following linear relationship:

$$C^{\star\star}_{\mathrm{doc}}(t, x, z) = K_h\, C^{\star}_{\mathrm{doc}}(t, x, z) \tag{55}$$

where $C^{\star\star}_{\mathrm{doc}}(t, x, z)$ is the solute-humic concentration sorbed onto the solid matrix, the solute-humic substances retardation factor, R_{sh}, is defined as

$$R_{sh} = R_h = 1 + \frac{\rho_b\, K_h}{\theta} \tag{56}$$

Note that the partition coefficient for solute-humic substances between the solid matrix and the aqueous phase, K_h, is identical to the partition coefficient for humic substances between the solid matrix and the aqueous phase. Furthermore, it was assumed that solute-humic substances share the same transport properties as humic substances, because humic substances are much larger than solutes and that sorption of nonpolar compounds onto humic substances most likely does not significantly affect the sorption characteristics of humic macromolecules. Also, it was assumed that the decay of solute-humic substances is dictated by the decay of the solute. Therefore, $D_{x_h}=D_{x_{sh}}$, $D_{z_h}=D_{z_{sh}}$, and $\lambda_{sh}=\lambda_s$.

The appropriate initial and boundary conditions for the transport of solute-humic substances in the two-dimensional, homogeneous, water saturated formation considered here are the following:

$$\partial C^{\star}_{\mathrm{doc}}(0, x, z) = 0 \tag{57}$$

$$\frac{\partial C^{\star}_{\mathrm{doc}}(t, \pm\infty, z)}{\partial x} = \frac{\partial C^{\star}_{\mathrm{doc}}(t, x, \infty)}{\partial z} = \frac{\partial C^{\star}_{\mathrm{doc}}(t, x, 0)}{\partial z} = 0 \tag{58}$$

5.2 Numerical Model Simulations

The numerical solution for the solute-humic cotransport model was obtained by an unconditionally stable, fully implicit finite difference discretization method. The three governing transport Eqs. (38), (48), and (54) in conjunction with the initial and boundary conditions given by Eqs. (39)–(41), (51)–(53), (58) and (59) were solved simultaneously [57]. All flux boundary conditions were estimated using a second-order accurate one sided approximation [53].

Model simulations were performed in order to examine the effect of humic substances on the effective average mass transfer coefficient. The behavior of $\bar{k}_e$, defined in Eq. (47), as a function of time in the presence and absence of humic substances is illustrated in Fig.9a. Note that the parameter $L_h$is set equal to zero when dissolved humic substances are not present. Clearly, the results indicate that the presence of humic substances increases the mass transfer from the PCE pool into the aqueous phase. An increase in the mass transfer coefficient leads to faster dissolution of the PCE pool.

To illustrate further the effects of humic substances on NAPL pool solubility enhancement, dissolved PCE concentrations as a function of time were determined for an arbitrary point within the aquifer with coordinates x=39.2 cm and z=1.0 cm. The results are presented in Fig. 9b. The total PCE concentration represents the sum of the PCE sorbed onto doc, $C^{\star}_{\mathrm{doc}}$, and the aqueous PCE concentration, C. The doc ($\times 10^{-1}$) concentration is also presented in Fig. 9b. As the dissolved humic substances pass over the PCE-water interface, PCE dissolution is enhanced due to sorption of the dissolved contaminant onto suspended humic substances. However, the aqueous phase contaminant concentration at the pool-water interface is assumed to remain equal to C_s. When contami-

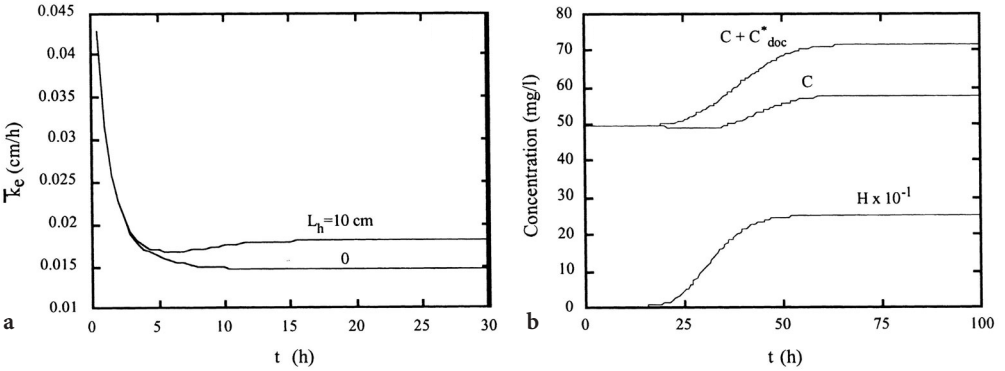

Fig. 9a, b Variation of the effective average mass transfer coefficient with increasing time evaluated for a PCE pool in the presence (L_h=10 cm) and absence (L_h=0 cm) of humic substances. **b** Breakthrough curves of the aqueous phase PCE concentration, C, total PCE concentration, $C+C^*_{doc}$, and doc concentration, H, at a point within the aquifer with coordinates x=39.2 cm, z=1 cm (here C_s=150 mg/l, D_{e_s}=0.0219 cm^2/h, D_{e_h}=0.009 cm^2/h, D_{x_s}=1.222 cm^2/h, D_{x_h}=1.209 cm^2/h, D_{z_s}=0.622 cm^2/h, D_{z_h}=0.609 cm^2/h, H_0=250 mg doc/l, K_d=0.310 l/kg dry solids, K_{doc}=9.56×10^{-4} l/mg doc, K_h=0.117 l/kg dry solids, ℓ_x=8.0 cm, ℓ_{x_o}=7.2 cm, L_h=10 cm, U_x=2.0 cm/h, α_x=0.6 cm, α_z=0.3 cm, ρ_b=1.47 g/cm^3, and θ=0.40)

nant-humic substances travel through sections of the aquifer with low aqueous phase contaminant concentrations, the contaminant desorbs from suspended humic substances into the aqueous phase, thus increasing the aqueous phase contaminant concentration. The concentration of PCE sorbed onto dissolved humic substances is the difference between the total PCE concentration and the aqueous phase PCE concentration.

6
Mass Transfer Correlations

Numerous empirical correlations for the prediction of residual NAPL dissolution have been presented in the literature and have been compiled by Khachikian and Harmon [68]. On the other hand, just a few correlations for the rate of interface mass transfer from single-component NAPL pools in saturated, homogeneous porous media have been established, and they are based on numerically determined mass transfer coefficients [69, 70]. These correlations relate a dimensionless mass transfer coefficient, i.e., Sherwood number, to appropriate Peclet numbers, as dictated by dimensional analysis with application of the Buckingham Pi theorem [71, 72], and they have been developed under the assumption that the thickness of the concentration boundary layer originating from a dissolving NAPL pool is mainly controlled by the contact time of groundwater with the NAPL-water interface that is directly affected by the interstitial groundwater velocity, hydrodynamic dispersion, and pool size. For uniform

groundwater flow, the velocity boundary layer can be ignored. Therefore, fluid properties such as dynamic viscosities and densities for both groundwater and NAPL do not contribute to the formation of the concentration boundary layer.

The three-dimensional mathematical model presented by Eqs. (7), (10)–(12), (14) and

$$C(t, x, y, 0) = C_s \qquad x, y \in R_{(r)} \text{ or } R_{(e)}, \tag{59a}$$

$$\frac{\partial C(t, x, y, 0)}{\partial z} = 0 \qquad x, y \notin R_{(r)} \text{ or } R_{(e)} \tag{59b}$$

where $R_{(r)}$ and $R_{(e)}$ are the domains for rectangular and elliptic pool-water interfacial areas, defined as

$$R_{(r)} : \ell_{x_o} \le x \le \ell_{x_o} + \ell_x \quad \text{and} \quad \ell_{y_o} \le y \le \ell_{y_o} + \ell_y, \tag{60}$$

$$R_{(e)} : \frac{(x - \ell_{x_o})^2}{a^2} + \frac{(y - \ell_{y_o})^2}{b^2} \le 1, \tag{61}$$

respectively, was solved numerically by an alternating direction implicit (ADI) finite-difference scheme. It should be noted that a circular pool with radius r is just a special case of an elliptic pool; therefore, the appropriate source boundary condition for a circular pool is obtained by setting $a=b=r$.

6.1 Local Mass Transfer Correlations

Chrysikopoulos and Kim [70] developed time invariant, local mass transfer correlations for NAPL pool dissolution in saturated media based on numerically determined local mass transfer coefficients evaluated for interstitial fluid velocities of 0.1, 0.5, 0.7, 0.85, and 1.0 m/day. It should be noted that solubility concentrations may occur at a NAPL-water interface when interstitial fluid velocities are less than 1.0 m/day [8]. Over 200 different rectangular pools with dimensions $\ell_x \times \ell_y$ in the range from 0.2 m×0.2 m to 10.0 m×10.0 m and approximately the same number of elliptic/circular pools with semiaxes $a \times b$ in the range 0.1 m×0.1 m to 5.0 m×5.0 m were examined.

6.1.1 Rectangular Pools

The fundamental parameters that affect mass transfer from a single component rectangular NAPL pool are the interstitial fluid velocity, effective molecular diffusion, dispersion coefficients, local coordinates of a specific location at the NAPL-water interface, and the square root of the rectangular pool area, $\ell_{c(r)}$, representing a characteristic length. The time invariant local mass transfer coefficient for a single component rectangular NAPL pool can be represented by the following functional relationship:

$$\hat{k}(x', y') = f[U_x, D_e, D_x, D_y, x', y', \ell_{c(r)}], \tag{62}$$

where

$$x' = x - \ell_{x_o}, \tag{63}$$

$$y' = y - \left(\ell_{y_o} + \frac{\ell_y}{2}\right) \tag{64}$$

$$\ell_{c(r)} = (\ell_x \ell_y)^{1/2}, \tag{65}$$

f is an arbitrary function, and x' and y' represent the shifted coordinate system. Using dimensional analysis, Chrysikopoulos and Kim [70] have shown that for rectangular NAPL pools the local Sherwood number is related to appropriate local Peclet numbers as follows:

$$Sh_{(r)}(x', y') = \beta_1 \, Pe_{x(r)}^{\beta_2} \, Pe_{y(r)}^{\beta_3} \tag{66}$$

where

$$Sh_{(r)} = \frac{\hat{k}(x', y')\, x', y'}{D_e \, \ell_{c(r)}} \tag{67}$$

$$Pe_{x(r)} = \frac{U_x \, x'}{D_x} \tag{68}$$

$$Pe_{y(r)} = \frac{U_x \, y'}{D_y} \tag{69}$$

$$\beta_1 = 0.01 \; \ell_x^{-0.53} (\ell_y/2)^{1.16} \; U_x^{-0.11}, \tag{70}$$

$$\beta_2 = 0.69 \; \ell_x^{0.13} \; U_x^{0.04}, \tag{71}$$

$$\beta_3 = 1.35 \, (\ell_y/2)^{-0.55} \; U_x^{0.01}, \tag{72}$$

where the subscript (r) designates a rectangular pool. The Sherwood number, $Sh_{(r)}$, is defined as the rate of interface mass transfer resistance to molecular diffusion resistance that physically represents the dimensionless concentration gradient at the NAPL-water interface. The local Peclet numbers, $Pe_{x(r)}$ and $Pe_{y(r)}$, represent the advective-dispersive mass transfer in the x and y directions, respectively. The correlation coefficients β_1, β_2, and β_3 were determined by fitting Eq. (66) to Sherwood numbers evaluated by numerically estimated $\hat{k}(x', y')$ values for various hydrodynamic conditions. It should be noted that unlike overall Sherwood number correlations with constant coefficients which are often published in the literature, Eq. (66) is a proposed empirical relationship for the local Sherwood number. Therefore, the local empirical coefficients are shown to depend on pool geometry and hydrodynamic conditions. The Eqs. (70)–(72) are valid for groundwater velocities in the range from 0.1 to 1.0 m/d and rectangular pools with dimensions $\ell_x \times \ell_y$ in the range from 0.2 m×0.2 m to 10.0 m×10.0 m.

6.1.2 Elliptic/Circular Pools

For a single component elliptic/circular NAPL pool the fundamental parameters that affect the local mass transfer coefficient are the same as those listed for the case of a rectangular pool. Therefore, the time invariant local mass transfer coefficient for a single component elliptic NAPL pool can be represented by the following functional relationship:

$$\hat{k}(x', y') = f[U_x, D_e, D_x, D_y, x', y', \ell_{c(e)}], \tag{73}$$

where

$$x' = x - \ell_{x_o}, \tag{74}$$

$$y' = y - \ell_{y_o}, \tag{75}$$

$$\ell_{c(e)} = (\pi ab)^{1/2}, \tag{76}$$

x' and y' represent the coordinates of the Cartesian coordinate system with the origin shifted to the center of the elliptic pool, and $\ell_{c(e)}$ is the corresponding characteristic length that represents the square root of the elliptic pool area. Using dimensional analysis, Chrysikopoulos and Kim [70] have shown that for elliptic NAPL pools the local Sherwood number is related to appropriate local Peclet numbers as follows:

$$Sh_{(e)}(x', y') = \gamma_1 \, Pe_{x(e)}^{\gamma_2} \, Pe_{y(e)}^{\gamma_3}, \tag{77}$$

where

$$Sh_{(e)} = \frac{\hat{k}(x', y')|x'|\, y'}{D_e \, \ell_{c(e)}} \tag{78}$$

$$Pe_{x(e)} = \frac{U_x |x'|}{D_x}, \tag{79}$$

$$Pe_{y(e)} = \frac{U_x \, y'}{D_y}, \tag{80}$$

$$\gamma_1 = 0.10 \, (2a)^{-3.26} \, b^{-1.51} \, U_x^{-1.21}, \tag{81}$$

$$\gamma_2 = 5.31 \, (2a)^{0.27} \, b^{-0.20} \, U_x^{0.21}, \tag{82}$$

$$\gamma_3 = 7.65 \, (2a)^{0.10} \, b^{-0.19} \, U_x^{0.24}, \tag{83}$$

and the subscript (e) designates an elliptic/circular pool, and $|x'|$ is the absolute value of the distance from the center of the pool along the flow direction. The correlation coefficients γ_1, γ_2, and γ_3 were determined by fitting Eq. (77) to Sherwood numbers evaluated by numerically estimated $\hat{k}(x', y')$ values for various hydrodynamic conditions. The correlation presented can be applied to circular

pools by setting $a=b=r$. The Eqs. (81)–(83) are valid for groundwater velocities in the range from 0.1 to 1.0 m/d and elliptic/circular NAPL pools with semiaxes $a\times b$ in the range from 0.1 m×0.1 m to 5.0 m×5.0 m.

6.2 Average Mass Transfer Correlations

Kim and Chrysikopoulos [69] developed time invariant, average mass transfer correlations for NAPL pool dissolution in saturated media, based on numerically determined average mass transfer coefficients evaluated for interstitial fluid velocities of 0.3, 0.5, 0.7, and 1.0 m/day. It should be noted that the dimensionless retardation factor R was arbitrarily set to 1.0, because at steady state conditions concentration profiles for a nondecaying solute are no longer dependent on R [24]. The dispersion coefficients D_x, D_y, and D_z were chosen in the range from 2.5–8.3×10^{-2} m^2/h, 2.5–8.3×10^{-3} m^2/h and 2.5–8.3×10^{-3} m^2/h, respectively. A total of 121 different rectangular pools with dimensions $\ell_x\times\ell_y$ in the range from 5.0 m×5.0 m to 10.0 m×10.0 m, and 121 different elliptic/circular pools with semiaxes $a\times b$ in the range 2.5×2.5 m to 5.0×5.0 m were examined.

6.2.1 Rectangular Pools

The time invariant, average mass transfer coefficient of a single component rectangular NAPL pool can be expressed by the following functional relationship:

$$k^\star = f[U_x, D_e, D_x, D_y, \ell_x, \ell_y, \ell_{c(\mathrm{r})}]. \tag{84}$$

Kim and Chrysikopoulos [69] have shown that for rectangular NAPL pools the average Sherwood number is related to appropriate average Peclet numbers as follows:

$$Sh^\star_{(\mathrm{r})} = \beta_1 (Pe^\star_{x(\mathrm{r})})^{\beta 2} (Pe^\star_{y(\mathrm{r})})^{\beta 3}, \tag{85}$$

where

$$Sh^\star_{(\mathrm{r})} = \frac{k^\star\, \ell_{c(\mathrm{r})}}{D_e}, \tag{86}$$

$$Pe^\star_{x(\mathrm{r})} = \frac{U_x\, \ell_x}{D_x}, \tag{87}$$

$$Pe^\star_{y(\mathrm{r})} = \frac{U_x\, \ell_y}{D_y}, \tag{88}$$

β_1, β_2, and β_3 are empirical coefficients that were determined by fitting the nonlinear power law correlation Eq. (85) to 484 average Sherwood numbers com-

puted for 121 different pool dimensions and four different sets of hydrodynamic conditions. The resulting time invariant, average mass transfer correlation for rectangular pools is given by

$$Sh^{\star}_{(\mathrm{r})} = 1.58\,(Pe^{\star}_{x(\mathrm{r})})^{0.34}\,(Pe^{\star}_{y(\mathrm{r})})^{0.43} \tag{89}$$

This correlation is valid for groundwater velocities in the range from 0.1 to 1.0 m/d, and rectangular NAPL pools with dimensions $\ell_x \times \ell_y$ in the range from 5.0 m×5.0 m to 10.0 m×10.0 m.

6.2.2 Elliptic/Circular Pools

The time invariant, average mass transfer coefficient of a single component elliptic NAPL pool can be expressed by the following functional relationship:

$$k^{\star} = f[U_x, D_e, D_x, D_y, \ell_x, \ell_y, \ell_{c(\mathrm{e})}]. \tag{90}$$

Kim and Chrysikopoulos [69] have shown that for elliptic NAPL pools the average Sherwood number is related to appropriate average Peclet numbers as follows:

$$Sh^{\star}_{(\mathrm{e})} = \gamma_1\,(Pe^{\star}_{x(\mathrm{e})})^{\gamma 2}\,(Pe^{\star}_{y(\mathrm{e})})^{\gamma 3}, \tag{91}$$

where

$$Sh^{\star}_{(\mathrm{e})} = \frac{k^{\star}\,\ell_{c(\mathrm{e})}}{D_e}, \tag{92}$$

$$Pe^{\star}_{x(\mathrm{e})} = \frac{U_x\,a}{D_x}, \tag{93}$$

$$Pe^{\star}_{y(\mathrm{e})} = \frac{U_x\,b}{D_y}, \tag{94}$$

γ_1, γ_2, and γ_3 are empirical coefficients that were determined by fitting the nonlinear power law correlation Eq. (91) to 484 average Sherwood numbers computed for 121 different pool dimensions and four different sets of hydrodynamic conditions. The resulting time invariant, average mass transfer correlation for elliptic pools is given by

$$Sh^{\star}_{(\mathrm{e})} = 1.74(Pe^{\star}_{x(\mathrm{e})})^{0.33}\,(Pe^{\star}_{y(\mathrm{e})})^{0.40} \tag{95}$$

This correlation can be applied to circular pools by setting $a=b=r$. It should be noted that the Eq. (95) is valid for groundwater velocities in the range from 0.1 to 1.0 m/d, and elliptic/circular pools with semiaxes $a \times b$ in the range 2.5×2.5 m to 5.0×5.0 m.

7
Experimental Studies of NAPL Pool Dissolution in Porous Media

Chrysikopoulos et al. [73] designed and constructed a unique three-dimensional, bench-scale model aquifer to carry out DNAPL pool dissolution experiments. The model aquifer was constructed by glass with a specially designed aluminum bottom plate. A 0.5 cm deep, circular disk with 7.6 cm diameter was removed from the aluminum sheet in order to form the experimental pool. Glass beads were placed in the pool in order to support a #60 stainless steel mesh that prevented settling of sand into the pool. A 16 gauge stainless tube inserted into the pool through a horizontal hole drilled along the aluminum sheet was used to deliver the trichloroethylene (TCE) into the experimental pool. The aquifer material was well-characterized, uniform sand kiln-dried Monterey sand (RMC Lonestar, Monterey, California). The aqueous phase pumped through the experimental aquifer was degassed, deionized water with sodium azide. A schematic diagram of the three-dimensional, bench-scale model aquifer and a blowup of the sampling plate is shown in Fig. 10. It should be noted that a total

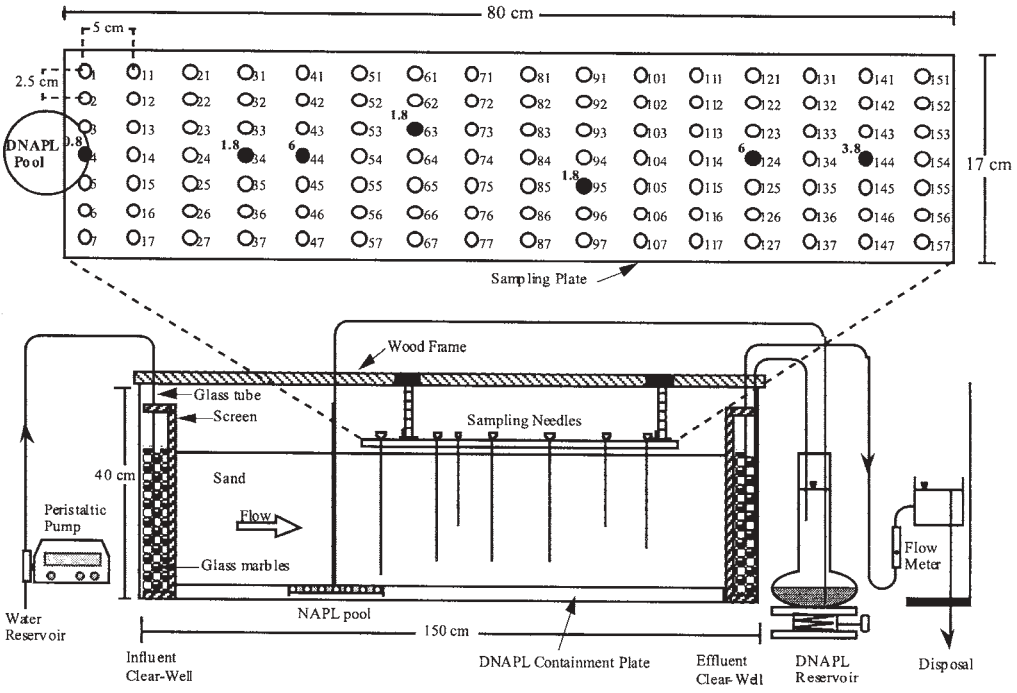

Fig. 10 Schematic diagram of the experimental aquifer and the sampling plate. *Filled circles* on the sampling plate represent needle placement locations. For each *filled circle*, the *lower right number* indicates the sampling port number and the *upper left bold numbers* indicate the needle placement depth measured in cm from the bottom of the aquifer (adopted from Lee and Chrysikopoulos [74])

of seven needles were vertically inserted into the aquifer and their locations are indicated on the sampling plate as filled circles. The designation of each sampling port is specified in Fig. 10 by a lower right number; whereas, the needle placement depth, measured in centimeters from the bottom of the aquifer, is indicated by a bold number at the upper left side of each sampling port.

The characteristics of the experimental aquifer were independently determined from appropriate flowthrough column experiments or obtained directly from the literature. The dry bulk density of the sand ρ_b=1.61 kg/l, and the aquifer porosity θ=0.415 were evaluated by gravimetric procedures. The dimensionless retardation factor, R=1.31, of the aqueous-phase TCE was determined from a column flowthrough experiment. The tortuosity coefficient for the aquifer sand was considered to be τ^*=1.43 [75]. The molecular diffusion coefficient for the aqueous-phase TCE is D=0.0303 cm^2/h [76]. The pool radius is r=3.8 cm. Bromide ion in the form of the moderately soluble potassium bromide salt was the tracer of choice [77] for the tracer experiment conducted in order to determine the longitudinal and transverse aquifer dispersivities α_L=0.259 cm and α_T= 0.019 cm, respectively. The experimental pool contained approximately 12 ml of certified ACS grade (Fisher Scientific) TCE with solubility of C_s=1100 mg/l [78].

7.1 TCE Dissolution Data

The experimental aqueous-phase TCE concentrations at specific locations within the aquifer downstream from the TCE pool for seven different interstitial fluid velocities (0.25, 0.51, 0.75, 1.21, 1.50, 1.96, and 3.35 cm/h) and steady-state conditions were collected by Chrysikopoulos et al. [73] and Lee and Chrysikopoulos [74]. For each TCE dissolution experiment, samples were simultaneously collected from sampling ports 4 (located at x=0.0, y=0.0, z=0.8 cm), 34 (15.0, 0.0, 1.8), 63 (30.0, 2.5, 1.8), 95 (45.0, –2.5, 1.8), and 144 (70.0, 0.0, 3.8). It should be noted that the origin of the Cartesian coordinate (0,0,0) is directly below port 4, and the center of the circular TCE pool is located at (–3.8,0,0). The interstitial velocity in the aquifer was altered by changing the water volumetric flow rate of the peristaltic pump. Aqueous phase TCE concentrations were collected only when steady state concentrations were observed at sampling port 144, that is the sampling port farthest away from the TCE pool (see Fig. 10). The duplicate aqueous phase TCE concentration experimental data were averaged and presented in Fig. 11. The experimental data indicate that aqueous phase TCE concentrations decrease with increasing U_x. This trend of the TCE concentration data was expected because the concentration boundary layer decreases with increasing interstitial velocity [30]. For each U_x considered, the highest dissolved concentration was observed at sampling port 4, that is closest to the TCE pool, and the lowest dissolved concentration was observed at node 144, that is the farthest away from the pool.

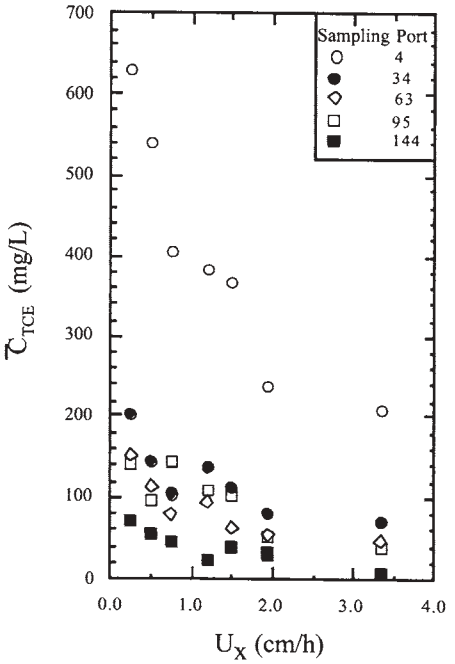

Fig. 11 Observed steady-state aqueous-phase TCE concentrations as a function of interstitial velocity at five different sampling ports (adopted from Lee and Chrysikopoulos [74])

7.2 Experimental Mass Transfer Correlation

For each set of aqueous-phase TCE concentrations collected, the corresponding k^* was estimated by fitting the analytical solution for a circular NAPL pool given by Eq. (21) to the experimental data with the non-linear least squares regression program PEST [79]. The estimated time invariant mass transfer coefficients together with the corresponding 95% confidence intervals, as determined by PEST, are presented in Fig. 12a. Clearly, it is shown that k^* increases steadily with increasing U_x. It should be noted that as U_x continues to increase, k^* approaches an asymptotic value.

The nonlinear least squares regression program PEST [79] was used to fit the proposed correlation relating the time invariant Sherwood number to overall Peclet numbers for circular pools given by Eq. (91) to the seven experimentally determined Sh^* values presented in Fig. 12b, in order to estimate the empirical coefficients γ_1, γ_2, and γ_3. The experimental, overall Sherwood number correlation applicable to circular TCE pool dissolution in water saturated, homogeneous porous media can be expressed by the following relationship:

$$Sh^*_{(e)} = 1.30\,(Pe^*_x)^{0.12}\,(Pe^*_y)^{0.44} \tag{96}$$

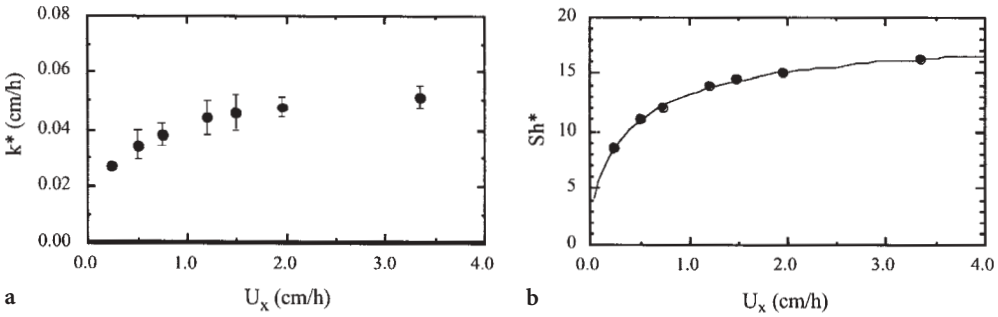

Fig. 12a, b Fitted time invariant overall mass transfer coefficients as a function of U_x evaluated from the averaged two sets of concentration measurements with error bars representing the 95% confidence intervals. **b** Comparison between experimentally determined *Sh** values (*solid circles*) and the experimental overall mass transfer correlation (*solid curve*) as a function of U_x

Figure 12b presents the experimentally determined correlation, Eq. (96), (solid curve) together with the experimentally determined *Sh** values (solid circles) as a function of interstitial velocity.

8 Summary

The fundamentals of mass flux at a NAPL-water interface within water saturated porous formations were discussed. Analytical solutions applicable for contaminant transport originating from NAPL pool dissolution in three-dimensional, homogeneous, water saturated porous media were presented for rectangular, elliptic as well as circular NAPL pools. The analytical solutions are useful for design and interpretation of experiments in laboratory-packed beds and possibly some homogeneous aquifers, and for the verification of complex numerical models. It was demonstrated through synthetic examples that the more elongated the pool along the direction of the interstitial flow, the higher the dissolved peak concentration. The effect of aquifer anisotropy and heterogeneity on the average mass transfer coefficient associated with DNAPL pool dissolution in water saturated porous media was examined with a numerical model. It was shown that increasing aquifer anisotropy results in an increase of the average mass transfer coefficient and that the average mass transfer coefficient is inversely proportional to the variance of the log-transformed hydraulic conductivity distribution. A two-dimensional finite difference numerical model was presented for the simulation of NAPL pool dissolution in a homogeneous, water saturated aquifer in the presence of dissolved humic substances. Model simulations indicated that dissolved humic substances may increase considerably NAPL pool dissolution. Local as well as average mass transfer correlations,

based on numerical data, describing the rate of the interface mass transfer from single component rectangular or elliptic/circular NAPL pools in water saturated, homogeneous porous media were presented. The mass transfer correlations relate dimensionless mass transfer coefficients (Sherwood numbers) to appropriate Peclet numbers and can be used in existing analytical or numerical mathematical models simulating the transport of dissolved organics originating from the dissolution of NAPL pools in water saturated subsurface formations. Furthermore, an average mass transfer correlation based on experimentally determined mass transfer coefficients obtained from a unique, bench-scale, three-dimensional, TCE pool dissolution experiment was presented.

References

1. Schwille F (1984) Migration of organic fluids immiscible with water in the unsaturated zone. In: Yaron B, Dagan G, Goldshmid J (eds) Pollutants in porous media: the unsaturated zone between soil surface and groundwater. Springer, Berlin Heidelberg New York, pp 27–48
2. Mackay DM, Cherry JA (1989) Groundwater contamination: pump-and-treat remediation. Environ Sci Technol 23(6):630–636
3. Seagren EA, Rittmann BE, Valocchi AJ (1994) Quantitative evaluation of the enhancement of NAPL-pool dissolution by flushing and biodegradation. Environ Sci Technol 28:833–839
4. Schwille F (1981) Groundwater pollution in porous media by fluids immiscible with water. In: van Diujvenbooden W, Glasberger P, Lelyveld HH (eds) Quality of groundwater, studies in environmental science, vol 17. Elsevier Science, New York, NY, pp 451–463
5. Anderson MR, Johnson RL, Pankow JF (1992) Dissolution of dense chlorinated solvents into groundwater. 3. Modeling contaminant plumes from fingers and pools of solvent. Environ Sci Technol 26:901–908
6. Schwille F (1988) Dense chlorinated solvents in porous and fractured media. Translated by Pankow JF. Lewis, Chelsea, Michigan
7. Mackay DM, Roberts PV, Cherry JA (1985) Transport of organic contaminants in groundwater. Environ Sci Technol 19:364–392
8. Powers SE, Loureiro CO, Abriola LM, Weber WJ Jr (1991) Theoretical study of the significance of nonequilibrium dissolution of nonaqueous phase liquids in subsurface systems. Water Resour Res 27:463–477
9. Fried JJ, Muntzer P, Zilliox L (1979) Ground-water pollution by transfer of oil hydrocarbons. Ground Water 17:586–594
10. Abriola LM, Pinder GF (1985) A multiphase approach to the modeling of porous media contamination by organic compounds. 1. Equation development. Water Resour Res 21:11–18
11. Powers SE, Abriola LM, Weber WJ Jr (1992) An experimental investigation of nonaqueous phase liquid dissolution in saturated subsurface systems: seady state mass transfer rates. Water Resour Res 28:2691–2705
12. Thomson NR, Graham DN, Farquhar GJ (1992) One-dimensional immiscible displacement experiments. J Contam Hydrol 10:197–223
13. Lenhard RJ, Johnson TG, Parker JC (1993) Experimental observations of nonaqueous phase liquid subsurface movement. J Contam Hydrol 12:79–101
14. Pantazidou M, Sitar N (1993) Emplacement of nonaqueous liquids in the vadose zone. Water Resour Res 29:705–722

15. Imhoff PT, Jaffé PR, Pinder GF (1994) An experimental study of complete dissolution of a nonaqueous phase liquid in saturated porous media. Water Resour Res 30:307–320
16. Powers SE, Abriola LM, Weber WJ Jr (1994) An experimental investigation of nonaqueous phase liquid dissolution in saturated subsurface systems: Transient mass transfer rates. Water Resour Res 30:321–332
17. Bear J, Ryzhik V, Braester C, Entov V (1996) On the movement of an LNAPL lens on the water table. Transp Porous Media 25:283–311
18. Keller AA, Blunt MJ, Roberts PV (1997) Micromodel observation of the role of oil layers in three-phase flow. Transp. Porous Media 26:277–297
19. Kennedy CA, Lennox WC (1997) A pore-scale investigation of mass transport from dissolving DNAPL droplets. J Contam Hydrol 24:221–244
20. Jia C, Shing K, Yortsos YC (1999) Advective mass transfer from stationary sources in porous media. Water Resour Res 35:3239–3251
21. Brusseau ML, Nelson NT, Oostrom M, Zhang Z, Johnson GR, Wietsma TW (2000) Influence of heterogeneity and sampling method on aqueous concentrations associated with NAPL dissolution. Environ Sci Technol 34:3657–3664
22. Zhou D, Dillard LA, Blunt MJ (2000) A physically based model of dissolution of nonaqueous phase liquids in the saturated zone. Transp Porous Media 39:227-255
23. Johnson RL, Pankow JF (1992) Dissolution of dense chlorinated solvents into groundwater. 2. Source functions for pools of solvent. Environ Sci Tech 26:896–901
24. Chrysikopoulos CV, Voudrias EA, Fyrillas MM (1994) Modeling of contaminant transport resulting from dissolution of nonaqueous phase liquid pools in saturated porous media. Transp Porous Media 16:125–145
25. Voudrias EA, Yeh MF (1994) Dissolution of a toluene pool under constant and variable hydraulic gradients with implications for aquifer remediation. Groundwater 32:305–311
26. Lee KY, Chrysikopoulos CV (1995) Numerical modeling of three-dimensional contaminant migration from dissolution of multicomponent NAPL pools in saturated porous media. Environ Geol 26:157–165
27. Lee KY, Chrysikopoulos CV (1998) NAPL pool dissolution in stratified and anisotropic porous formations. J Environ Eng ASCE 124:851–862
28. Holman H-YN, Javandel I (1996) Evaluation of transient dissolution of slightly water-soluble compounds from a light nonaqueous phase liquid pool. Water Resour Res 32: 915–923
29. Mason AR, Kueper BH (1996) Numerical simulation of surfactant-enhanced solubilization of pooled DNAPL. Environ Sci Technol 30:3205–3215
30. Chrysikopoulos CV, Lee KY (1998) Contaminant transport resulting from multicomponent phase liquid pool dissolution in three-dimensional subsurface formations. J Contam Hydrol 31:1–21
31. Seagren EA, Rittmann BE, Valocchi AJ (1999) An experimental investigation of NAPL pool dissolution enhancement by flushing. J Contam Hydrol 37:111–137
32. Leij FJ, van Genuchten MT (2000) Analytical modeling of nonaqueous phase liquid dissolution with Green's functions. Transp Porous Media 38:141–166
33. Leij FJ, Priesack E, Schaap MG (2000) Solute transport modeled with Green's functions with application to persistent solute sources. J Contam Hydrol 41:155–173
34. Sciortino A, Harmon TC, Yeh W-G (2000) Inverse modeling for locating dense nonaqueous pools in groundwater under steady flow conditions. Water Resour Res 36: 1723–1735
35. Parker JC, Katyal AK, Kaluarachchi JJ, Lenhard RJ, Johnson TJ, Jayaraman K, Ünlü K, Zhu JL (1991) Modeling multiphase organic chemical transport in soils and groundwater. US Environmental Protection Agency Project CR-814320, Washington D.C., USA

36. Pinder GF, Abriola LM (1986) On the simulation of nonaqueous phase organic compounds in the subsurface. Water Resour Res 22:109s–119s
37. van der Waarden M, Bridie ALAM, Groenewoud WM (1971) Transport of mineral oil components to groundwater. 1. Model experiments on the transfer of hydrocarbons from a residual oil zone to trickling water. Water Res 5:213–226
38. Borden RC, Kao C-M (1992) Evaluation of groundwater extraction for remediation of petroleum-contaminated aquifers. Water Environ Res 64:28–36
39. Borden RC, Piwoni MD (1992) Hydrocarbon dissolution and transport-A comparison of equilibrium and kinetic models. J Contam Hydrol 10:309–323
40. Chrysikopoulos CV (1995) Three-dimensional analytical models of contaminant transport from nonaqueous phase liquid pool dissolution in saturated subsurface formations. Water Resour Res 31:1137–1145
41. Incropera FP, DeWitt DP (1990) Fundamentals of heat and mass transfer. Wiley, New York, NY, p 919
42. Bear J, Verruijt A (1987) Modeling groundwater flow and pollution. D. Reidel, Dordrecht, Holand, p 414
43. Hashimoto I, Deshpande KB, Thomas HC (1964) Peclet numbers and retardation factors for ion exchange columns. Ind Eng Chem Fund 3:213–218
44. Vogler ET, Chrysikopoulos CV (2001) Dissolution of nonaqueous phase liquid pools in anisotropic aquifers. Stoch Environ Res Risk Assess 15:33–46
45. Gutjhar AL (1989) Fast Fourier transform for random field generation. Los Alamos Report 4-R58-2690R, New Mexico Institute of Mining and Technology, Socorro, NM
46. Gelhar LW, Axness CL (1983) Three-dimensional stochastic analysis of macrodisisperion in aquifers. Water Resour Res 19:161–180
47. Sudicky EA (1986) A natural gradient experiment on solute transport in a sand aquifer: spatial variability of hydraulic conductivity and its role in the disperion process. Water Resour Res 22:2069–2082
48. Russo D, Zaidel J, Laufer A (1994) Stochatic analysis of solute transport in partially saturated heterogeneous soils. 1. Numerical experiments. Water Resour Res 30:769–779
49. Burr DT, Sudicky EA, Naff RL (1984) Nonreactive and reactive solute transport in three-dimensional heterogeneous porous media: mean displacement, plume spreading, and uncertainty. Water Resour Res 30:791–815
50. Bear J (1979) Hydraulics of goundwater. McGraw-Hill, New York, NY
51. Freeze RA (1975) A stochastic-conceptual analysis of one-dimensional groundwater flow in nonuniform homogeneous media. Water Resour Res 11:725–741
52. Dagan G (1989) Flow and transport in porous formations. Springer, Berlin Heidelberg New York
53. Strikwerda JC (1989) Finite difference schemes and partial differential equations. Wadsworth & Brooks/Cole, Pacific Grove, CA
54. Smith L (1981) Spatial variability of flow parameters in a stratified sand. Math Geol 13:1–21
55. Larson RA, Weber EJ (1994) Reaction mechanisms in environmental organic chemistry. CRC Press, Raton, FL
56. Chiou CT, Malcolm RL, Brinton TI, Kile DE (1986) Water solubility enhancement of some organic pollutants and pesticides by dissolved humic and fulvic acids. Environ Sci Technol 20:502–508
57. Tatalovich ME, Lee KY, Chrysikopoulos CV (2000) Modeling the transport of contaminants originating from the dissolution of DNAPL pools in aquifers in the presence of dissolved humic substances. Transp Porous Media 38:93–115
58. Carter CW, Suffet IH (1982) Binding of DDT to dissolved humic materials. Environ Sci Technol 16:735–740

59. Chiou CT, Kile DE, Brinton TI, Malcolm RL, Leenheer JA (1987) A comparison of water solubility enhancements of organic solutes by aquatic humic materials and commercial humic acids. Environ Sci Technol 21:1231–1234
60. Chin Y-P, Weber WJ Jr (1989) Estimating the effects of dispersed organic polymers on the sorption of contaminants by natural solids. 1. A predictive thermodynamic humic substance-organic solute interaction mode. Environ Sci Technol 23:978–984
61. Abdul AS, Gibson TL, Rai DN (1990) Use of humic acid solution to remove organic contaminants from hydrogeologic systems. Environ Sci Technol 24:106–114
62. Kopinke R-D, Porschmann J, Stottmeister U (1995) Sorption of organic pollutants on anthropogenic humic matter. Environ Sci Technol 29:941–950
63. Tanaka S, Oba K, Fukushima M, Nakayasu K, Hasebe K (1997) Water solubility enhancement of pyrene in the presence of humic substances. Anal Chim Acta 337:351–357
64. Murphy EM, Zachara JM, Smith SC, Phillips JL (1992) The sorption of humic acids to mineral surfaces and their role in contaminant binding. Sci Total Environ 117:413–423
65. Liljestrand HM, Lo I, Shimizu Y (1992) Sorption of humic materials onto inorganic surfaces for the mitigation of facilitated pollutant transport processes. Water Sci Technol 26:1221–1228
66. Jardine PM, Dunnivant FM, Selim HM, McCarthy JF (1992) Comparison of models for describing the transport of dissolved organic carbon in aquifer columns. Soil Sci Soc Am J 56:393–401
67. McCarthy JF, Williams TM, Liang L, Jardine PM, Jolley LW, Taylor DL, Palumbo AV, Cooper LW (1993) Mobility of natural organic matter in a sandy aquifer. Environ Sci Technol 27:667–676
68. Khachikian C, Harmon TC (2000) Nonaqueous phase liquid dissolution in porous media: Current state of knowledge and research needs. Transp Porous Media 38:3–28
69. Kim T-J, Chrysikopoulos CV (1999) Mass transfer correlations for nonaqueous phase liquid pool dissolution in saturated porous media. Water Resour Res 35:449–459
70. Chrysikopoulos CV, Kim T-J (2000) Local mass transfer correlations for nonaqueous phase liquid pool dissolution in saturated porous media. Transp Porous Media 38:167–187
71. Bird RB, Stewart WE, Lightfoot EN (1960) Transport Phenomena. Wiley, New York, NY
72. Weber WJ Jr, DiGiano FA (1996) Process dynamics in environmental system. Wiley, New York, NY
73. Chrysikopoulos CV, Lee KY, Harmon TC (2000) Dissolution of a well-defined trichloroethylene pool in saturated porous media: experimental design and aquifer characterization. Water Resour Res 36:1687–1696
74. Lee KY, Chrysikopoulos CV (2002) Dissolution of a well-defined trichloroethylene pool in saturated porous media: experimental results and model simulations. Water Res 36:3911–3918
75. de Marsily G (1986) Quantitative hydrogeology, groundwater hydrology for engineers. Academic Press, San Diego, CA, pp 440
76. Hayduk W, Laudie H (1974) Prediction of diffusion coefficients for nonelectrolytes in dilute aqueous solutions. AIChE J 20:611–615
77. Chrysikopoulos CV (1993) Artificial tracers for geothermal reservoir studies. Environ Geology 22:60–70
78. Mackay D, Shiu WY, Ma KC (1992) Illustrated handbook of physical-chemical properties and environmental fate for organic chemicals, volatile organic chemicals, vol 3. Lewis, Chelsea, MI, pp 916
79. Doherty J, Brebber L, Whyte P (1994) PEST: Model-independent parameter estimation. Watermark Computing, Brisbane, Australia